Effect of O2(a1Δg) on the low-temperature mechanism of CH4 oxidation

ARTICLE *in* COMBUSTION AND FLAME · MARCH 2013

Impact Factor: 3.08 · DOI: 10.1016/j.combustflame.2012.11.020

Combustion and Flame xxx (2012) xxx–xxx

Contents lists available at SciVerse ScienceDirect

Combustion and Flame

journal homepage: www.elsevier.com/locate/combustflame

Effect of $O_2(a^1\Delta_g)$ on the low-temperature mechanism of CH_4 oxidation

Alexander Vladimirovich Lebedev [a,b,*], Maxim A. Deminsky [a,c], Andrey V. Zaitzevsky [a,c], Boris V. Potapkin [a,c]

[a] Kintech Lab, Kurchatov sq. 1, Moscow, Russia
[b] Moscow Institute of Physics and Technology, Institutsky per. 9, Dolgoprydny, Russia
[c] State Research Center RF Kurchatov Institute, Kurchatov sq. 1, Moscow, Russia

ARTICLE INFO

Article history:
Received 17 July 2012
Received in revised form 26 November 2012
Accepted 27 November 2012
Available online xxxx

Keywords:
Plasma
Combustion
Singlet oxygen
Hydrocarbon
Kinetics

ABSTRACT

The effect of electronically excited oxygen $O_2(a^1\Delta_g)$ on the combustion of methane in air at low temperatures is investigated. Sensitivity and rate of production analysis indicated that reactions $CH_3 + O_2(a^1\Delta_g) \leftrightarrow CH_3O_2(A')$; $CH_2O + OH$; $CH_3O + O$ are important for low-temperature methane oxidation. The potential energy surface of the reactions was investigated at the multi-reference configuration interaction level of theory. It was found that the association reaction corresponding to the channel of excited $CH_3O_2(A')$ formation has a threshold with an energy of 8.5 kcal/mole. The rate parameter of the reaction $CH_3 + O_2(a^1\Delta_g) \rightarrow CH_3O_2(A')$ was refined and makes $k = 2.76 \times 10^{-7} \times T^{-2.71} \times \exp\left(-\frac{8.61\ \text{kcal/mole}}{RT}\right)$. The influence of $O_2(a^1\Delta_g)$ on the rate of low-temperature methane oxidation in the refined model was analyzed. The study indicates significant suppression of the contribution of the channel $CH_3 + O_2(a^1\Delta_g) \rightarrow CH_3O_2$ due to peculiar properties of the potential energy surface of the reaction with participation of $O_2(a^1\Delta_g)$. At the same time, high contribution of the reaction channels leading to CH_2O and CH_3O results in effective use of the energy of electronic excitation for acceleration of the methane oxidation in presence of the $O_2(a^1\Delta_g)$ at low temperatures.

1. Introduction

Singlet oxygen $O_2(a^1\Delta_g)$ has lately become a subject of intense research [1–4] because of recent speculations on its capability of significantly enhancing the combustion of hydrocarbons, thus providing opportunities for the elaboration of new combustion-based devices and propulsion systems. Despite a great interest in excited oxygen and possible advantages of its use, detailed experimental research and understanding of the effect of singlet oxygen on the combustion of hydrocarbons [4] are still lacking. Even the combustion of the lightest hydrocarbons, e.g. methane, in the presence of singlet oxygen has not been a clear phenomena so far [1,3,5]. Although some efforts were made in modeling methane combustion involving singlet oxygen [1,6], a reliable theoretical model based on first-principles calculations is required. This study is devoted to a detailed theoretical analysis of important reaction pathways in the low-temperature oxidation of methane involving singlet oxygen.

The most interesting effect of $O_2(a^1\Delta_g)$ is the involvement of this molecule into the reactions of chain initiation and chain propagation. Such an active particle makes the most pronounced impact on the overall kinetics if it is concerned with the enhancement of rate-limiting reactions, which are mostly reactions with chemically stable species, i.e. initiation reactions. Another, and probably more significant option for $O_2(a^1\Delta_g)$, is the enhancement of the process due to participation in chain propagation reactions.

In the first case, $O_2(a^1\Delta_g)$ is mostly consumed by initiation reactions, leading to the multiplication of active radicals and hence, the reduction of the induction time. The second scenario is the enhancement of chain propagation reactions. The potential efficiency of $O_2(a^1\Delta_g)$ is higher for the second scenario, because each excited oxygen molecule could stimulate the production of a greater number of active radicals. However, the role of $O_2(a^1\Delta_g)$ in the chain propagation is not well elucidated, because the chain branched kinetics of hydrocarbon combustion (HC) is very sensitive to the variation of the rates of limiting stages. In particular, chain propagation enhanced by $O_2(a^1\Delta_g)$ can be the crucial stage in the kinetics of HC oxidation at relatively low temperatures ($T < 1000$ K), where the reaction with molecular oxygen

$$R^{\cdot} + O_2 \Longleftrightarrow ROO$$

and the subsequent reaction of chain propagation

$$ROO + RH \Longleftrightarrow ROOH + R^{\cdot}$$

are responsible for the switching of the oxidation mechanism between the chain initiation and chain branching kinetics [7]. At low temperatures, the shift of the reaction equilibrium towards

* Corresponding author at: Moscow Institute of Physics and Technology, Institutsky per. 9, Dolgoprydny, Russia. Fax: +7 499 196 78 37.
E-mail address: lebedev@kintechlab.com (A.V. Lebedev).

0010-2180/$ - see front matter © 2012 The Combustion Institute. Published by Elsevier Inc. All rights reserved.
http://dx.doi.org/10.1016/j.combustflame.2012.11.020

the chain branched mechanism and the acceleration of chain propagation may provide excited oxygen with an additional possibility for enhancing HC combustion. This effect could be achieved using, for example, cold non-equilibrium plasmas [1]. However, the problem formulated in such a way is a real challenge, as it requires accurate information about the rates of elementary processes involving $O_2(a^1\Delta_g)$. In fact, an inaccuracy of 5 kcal/mole in the energetic parameters of a reaction at temperatures below 900 K changes the reaction rate by about one order of magnitude and may become a reason for the incorrect conclusions about the pathways of oxidation in the mechanism.

Among the studies of the excited oxygen effect on the combustion kinetics, we can distinguish several works devoted to the combustion of hydrogen and light hydrocarbons. The influence of singlet oxygen on the hydrogen flame velocity was studied in Refs. [3,8].

A significant influence of singlet oxygen on combustion rate in hydrogen – air mixtures was reported in the works [2,8,9]. However, there are also studies indicating that the enhancement of combustion by excited oxygen is efficient only at relatively low temperatures and high concentrations of that species [3]. The optimization of discharge parameters for the efficient production of $O_2(a^1\Delta_g)$ was performed in the work [5]. It was shown that the presence of nitrogen significantly reduces the efficiency of $O_2(a^1\Delta_g)$ generation and required operation at high values of electric field strength.

A kinetic model of methane-air combustion in the presence of $O_2(a^1\Delta_g)$ was proposed in Refs. [1,6]. This model is focused on the behavior of ignition time and flame velocity at different concentrations of excited oxygen. The kinetic mechanism developed within this model was tested on a rich mixture, high temperatures ($T > 1600$ K), and homogeneous conditions with respect to induction time value and flame velocity. Since the flame velocity is determined by the processes occurring mainly at the flame front [10], there is no strong requirement for the accuracy of the rate characteristics, in contrast to what was mentioned before for low temperatures. Presumably, this is why reactions involving $O_2(a^1\Delta_g)$ are estimated within a rather rough "vibronic terms" model. Nevertheless, this model can be regarded as a basis for the comprehensive theoretical description of combustion process stimulated by $O_2(a^1\Delta_g)$.

Experimental studies of ethylene oxidation enhanced by $O_2(a^1\Delta_g)$ have recently been reported [4]. The effect of combustion enhancement by $O_2(a^1\Delta_g)$ was observed experimentally. However, the discrepancy between the experiment and theory indicates a lack of understanding of the role of elementary processes involving excited species and of knowledge about their parameters.

One of the key reactions of singlet oxygen in an air-methane mixture is the reaction with the methyl radical. Unfortunately, there are no experimental data on that process. Only several ab initio calculations of this reaction have been performed so far [11,12]. However, the difference in approaches used for calculations of the Potential Energy Surface (PES) for $CH_3 + O_2(a^1\Delta_g)$ may lead to a contradiction in the conclusions about the input of this reaction to the total oxidation mechanism. The difference in conclusions about the absence [12] or presence [11] of a threshold of the reaction together with the sufficiently great discrepancy for the excitation energies (26.3 kcal/mole, 24.6 kcal/mole) with respect to the table value (22.5 kcal/mole) makes the effect of the error propagation of ab initio calculations upon the final value of the oxidation rate at low temperatures strongly undetermined.

Thus, the accuracy of the models and calculations discussed above is not sufficient for making an unambiguous conclusion about the role of $O_2(a^1\Delta_g)$ in methane oxidation at low temperatures. The aim of this study was to find out the principal reactions involving excited oxygen, which provide the maximal sensitivity with respect to the overall kinetic parameters (induction time) and to evaluate the micro-kinetic characteristics of the key elementary reactions using state-of-the-art computational methods. The structure of the paper is the following. The first section is devoted to the analysis of the principal processes involving $O_2(a^1\Delta_g)$ based on the available kinetic mechanisms. Ab initio calculations of the rate parameters of the most important reactions with excited oxygen are discussed the in second part. The last section is the discussion of the results obtained.

2. $O_2(a^1\Delta_g)$ and the kinetics of methane oxidation

The effect of $O_2(a^1\Delta_g)$ on the kinetics of HC oxidation is not clear in details. Among the theoretical kinetic models of CH_4 oxidation, the model [1] seems the most developed and comprehended. To reveal the key elementary reactions involving excited oxygen at low temperatures, kinetic analysis was performed. The kinetic mechanism was composed of two parts. The first part is the methane combustion mechanism at low temperatures with reactions of species in the ground state [13,14]. The second part is the submechanism involving reactions of excited oxygen in accordance with the work mentioned above [1].

To select the most important processes with $O_2(a^1\Delta_g)$, a set of simulations with different initial conditions were performed using the Chemical Workbench (CWB) programs package [15]. The autoignition of a mixture CH_4:O_2:N_2 = 1:2:8 at a constant atmospheric pressure (Calorimetric Bomb Reactor model) and initial temperature range of 700–2000 K was simulated. The initial chemical composition corresponded to the combustion of a stoichiometric methane-air mixture. The effect of $O_2(a^1\Delta_g)$ was simulated by introducing an additional fraction of excited oxygen into the initial mixture. In different simulations the $O_2(a^1\Delta_g)$ concentration was varied in the range 0–10% of the initial concentration of $O_2(X^3\Sigma_g)$. The enhancement of the process by $O_2(a^1\Delta_g)$ was investigated by its influence on the induction time.

To find the key reactions responsible for the acceleration of oxidation by $O_2(a^1\Delta_g)$, the importance of reactions was analyzed using the Mechanism Reduction module of CWB [16,17]. Two approaches to reaction importance analysis were used. The first one was the sensitivity analysis of the OH radical to the reaction rate parameters. The sensitivity of the OH radical concentration to the reaction rate parameters shows the effect of variation of the rate parameter values with the concentration of active radicals. OH radical is one of the principal species which provide propagation of the chain oxidation process resulting in the ignition of the mixture [7]. Therefore sensitivity of OH was chosen as the indicator of the induction time sensitivity to the rate parameters of the reactions. Special attention should be payed to most sensitive reactions and rate parameters of such reactions are to be known with best precision in a reliable kinetic model. Table 1 presents the results of sensitivity analysis for the initial temperature 1000 K, atmospheric pressure, initial mixture CH_4:O_2:N_2 = 1:2:8, and initial $\frac{[O_2(a^1\Delta_g)]}{[O_2]} = 5\%$. The higher the magnitude of the sensitivity coefficient corresponding to a certain reaction, the greater the impact of a small variation of the corresponding rate parameter to the induction time of the process.

The second approach used for the analysis of the importance of reactions was the comparison of the relative rates of losses of $O_2(a^1\Delta_g)$ in different reactions integrated over the induction period of the reaction. The initial conditions for kinetic simulations were identical. Table 2 summarizes the results of analysis at different initial $O_2(a^1\Delta_g)$ concentrations.

Table 1 shows that the reaction of $O_2(a^1\Delta_g)$ with methyl corresponds to one of the highest values of sensitivity at the instant

Table 1
Sensitivity coefficients of [OH] to reaction rate parameters at different time moments of the process. T_{ini} = 1000 K, P = 1 atm, CH_4:O_2:N_2 = 1:2:8 and $O_2(a^1\Delta_g)$ = 5% O_2.

t, s	1e−5	1e−4	1e−3	1e−2	1e−1	$1 \sim t_{ind}$
$HO_2 + CH_3 \leftrightarrow OH + CH_3O$	0	0	0.075	1.6	0.55	11.4
$CH_3 + O_2(a^1\Delta_g) \rightarrow CH_3O_2$	0.055	0.057	0.07	0.54	1.6	7.64
$CH_3 + O_2(a^1\Delta_g) \rightarrow CH_3O + O$	0.43	0.61	0.88	1.34	0.01	0.82
$CH_3 + CH_3 + M \leftrightarrow C_2H_6 + M$	0	0	0.02	1.23	0.035	6.63
$CH_4 + O_2(a^1\Delta_g) \rightarrow CH_3 + HO_2$	1	1	1	0.4	0.013	0.15
$O_2(a^1\Delta_g) + H \rightarrow O + OH$	0.12	0.15	0.27	1	0.16	0.14
$OH + CH_4 \leftrightarrow CH_3 + H_2O$	0.84	1	1	0.95	1.03	1.84
$CH_2O + O_2(a^1\Delta_g) \rightarrow HCO + HO_2$	0	0	0	0.53	0.38	2.8

Table 2
Relative rate of $O_2(a^1\Delta_g)$ losses in several main reactions integrated over process time.

$\frac{[O_2(a^1\Delta_g)]}{[O_2]}$, %	2.5	5	7.5	10
$CH_3 + O_2(a^1\Delta_g) \rightarrow CH_3O_2$	0.49	0.35	0.28	0.34
$CH_2O + O_2(a^1\Delta_g) \rightarrow HCO + HO_2$	0.15	0.39	0.42	0.38
$CH_4 + O_2(a^1\Delta_g) \rightarrow CH_3 + HO_2$	0.36	0.24	0.2	0.23

close to the ignition moment. This reaction has several possible channels:

$$CH_3 + O_2(a^1\Delta_g) \rightarrow CH_3O_2(A') \quad (1a)$$
$$\rightarrow CH_2O + OH \quad (1b)$$
$$\rightarrow CH_3O + O \quad (1c)$$
$$\rightarrow HCO + H_2O \quad (1d)$$

which correlate with following channels of reaction of CH_3 with oxygen in the ground state:

$$CH_3 + O_2 \rightarrow CH_3O_2(A'') \quad (2a)$$
$$\rightarrow CH_2O + OH \quad (2b)$$
$$\rightarrow CH_3O + O \quad (2c)$$
$$\rightarrow HCO + H_2O \quad (2d)$$

In framework of used mechanism [1] the reactions (1a) and (2a) are the most important at low temperatures T < 800 K. The CH_3O_2 produced in these reactions may react with methane or HO_2 with further branching of oxidation process and multiplication of the active species and radicals [18]. At higher temperatures CH_3O_2 becomes a short-living intermediate and undergoes decay into either CH_3 and oxygen or CH_2O and OH.

Another sensitive reaction involving singlet oxygen is the initiation reaction:

$$CH_4 + O_2(a^1\Delta_g) \rightarrow CH_3 + HO_2 \quad (3)$$

corresponding to the reaction with oxygen in the ground state:

$$CH_4 + O_2 \rightarrow CH_3 + HO_2 \quad (4)$$

The sensitivity to this reaction is noticeable at early time moments, corresponding to the initiation of the combustion process. However, at the timescale when most of active radicals are generated, this reaction is not so sensitive.

According to Table 2, at low initial concentrations of $O_2(a^1\Delta_g)$ the reaction (1a) is the main channel of $O_2(a^1\Delta_g)$ losses (the highest value in the column). An increase in the initial concentration of excited oxygen provides conditions for the reaction of $O_2(a^1\Delta_g)$ with by-products. This effect leads to an increase in the contribution of channels involving other species, like CH_2O into the consumption of excited oxygen. However, these reactions do not affect induction time significantly according to sensitivity analysis (Table 1).

From the study of the crucial stages of low-temperature methane oxidation, we can conclude that the reaction (1a) is the key one for the reliable kinetic model of the process. The next sections will be devoted to the investigation of the potential energy surface of the system $CH_3 + O_2(a^1\Delta_g)$ and accurate evaluation of the rate parameters of low-temperature channels of this reaction.

Let us note that the above conclusion was made within of a uniform model. For strongly non-uniform systems, like flame, the peculiarity of coupling heat-mass transfer phenomena with chemical kinetics may change that statement [1].

3. Computational methods

3.1. Ab initio study of the reactions $CH_3 + O_2(X^3\Sigma;^1\Delta_g) \leftrightarrow CH_3O_2(^2A'';^2A')$

The Potential Energy Surface of the system $CH_3 + O_2(X^3\Sigma;\ ^1\Delta_g)$ was investigated at the multi-reference configuration interaction (MRCI) level of theory [19] in the triple-zeta basis set of Dunning and Hay. The geometry optimization and energy computations were performed with different CI active spaces. The initial approximations for both energies and geometries were taken from complete-active-space (CAS) calculations. The distance between the atoms C (of the CH_3 group) and O (of the O_2 group) was considered the reaction coordinate. Since the geometries of important points along the reaction coordinate were not known beforehand, the calculations were performed without a restriction by symmetry, although, in general, the system had a mirror plane given by the atoms C–O–O [11]. The ground term corresponded to the anti-symmetric wavefunction with respect to the symmetry plane ($^2A''$). On the contrary, the excited term belonged to the symmetric irreducible representation with respect to the symmetry plane ($^2A'$). The minimum of the potential well corresponded to the formation of a CH_3O_2 particle. The states $^2A''$ and $^2A'$ correlated with oxygen in the ground and excited state, respectively. Figures 1–3 present the geometries of CH_3O_2 ($^2A'$, $^2A''$) and the transition state.

To obtain MO orbitals and the initial approximations for geometries, the system was investigated using multiconfiguration

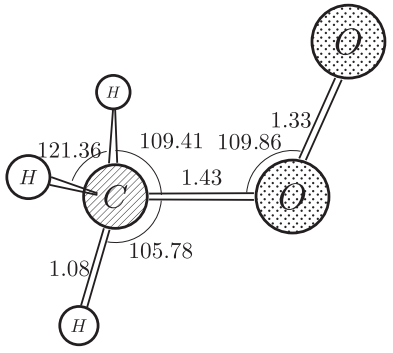

Fig. 1. Optimized geometry of $CH_3O_2(^2A'')$.

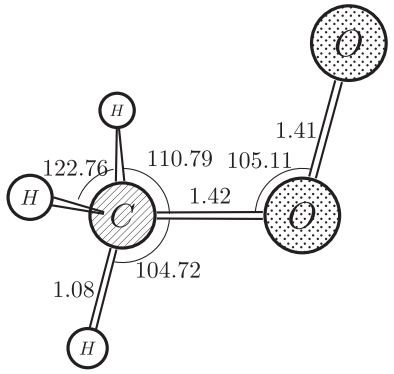

Fig. 2. Optimized geometry of $CH_3O_2(^2A')$.

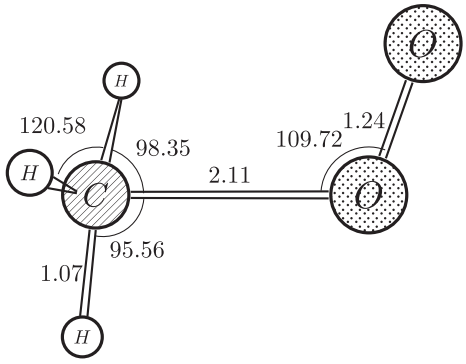

Fig. 3. Optimized geometry of the transition state for $CH_3O_2(^2A')$.

self-consistent-field calculations with an active space consisting of 9 electrons on 7 molecular orbitals MCSCF (9/7). The orbitals in the active space included a molecular orbital with an unpaired electron from the CH_3 group and 6 orbitals from the O_2 group. The following orbitals from the O_2 group were taken into account: bonding and antibonding σ orbitals formed by two 2p-orbitals of oxygen atoms and four bonding and antibonding π orbitals formed by 2p orbitals of oxygen atoms. The geometries and molecular orbitals were optimized in 10 points of the reaction coordinate between 1.5 Å and 5 Å at the MCSCF (9/7) level. The MCSCF wavefunction was optimized for the four lowest states.

To obtain accurate geometries and energies, the system was investigated at the MRCI level of theory with two different active space spans. The smaller active space consisted of 3 electrons on 4 molecular orbitals MRCI (3/4), while the largest one was MRCI (7/5). In the first case, the configuration corresponded to one orbital of the CH_3 group, two antibonding π orbitals corresponding to the O_2 group, and one antibonding σ orbital of the O_2 group. The doubly occupied space consisted of two bonding π, three lowest 2σ orbitals of the oxygen group, and two bonding π and one σ orbital of the CH_3 group.

Three lowest 1σ orbitals were placed to the frozen core. Several geometries spanning the reaction coordinate values from 1.4 Å to 5 Å were optimized with the reaction coordinate fixed at the MRCI (3/4) level of theory.

Three geometries were found to be important:

1. reaction coordinate 1.43 Å corresponding to the ground state of the CH_3O_2 particle.
2. reaction coordinate the for excited state of CH_3O_2 slightly less than that for the ground state.
3. reaction coordinate 2.1 Å corresponding to the transition state of the reaction (1a).

The reaction through the ground state (reaction (2a)) has no explicit form of the transition state (no threshold). Some previous studies of this reaction [20–22] have reported a potential barrier of 0.26–0.9 kcal/mole. Although we have also found a saddle point in the ground term between $CH_3 + O_2$ ($x^3\Sigma_g$) and $CH_3O_2(A'')$, the height of the barrier was very low and smoothed out by the following size-extensivity correction. Therefore, we can conclude that the barrier occurred in our study is due to the underestimation of electron correlation energy, which was corrected as discussed below.

The geometries of the important points were optimized without constraints on the coordinates of atoms. At the reaction coordinate equal to about 5 Å, the interaction between the methyl and oxygen groups vanished and they were considered separate fragments for both terms. Three lowest states were calculated at the MRCI level to achieve a better convergence of the two lowest states. Thus, the excited state $O_2(b^1\Sigma_g)$ was also included into the calculations and all possible correlations with it were taken into account.

To achieve better spanning of the active space, five important geometries were also optimized with the MRCI (7/5) and the energies for them were obtained. The active space was altered in the following manner: the antibonding σ orbital from oxygen was excluded from the virtual space, as it did not play noticeable role in the reaction. Instead of it two bonding π orbitals of the $O_2(a^1\Delta_g)$ group with four electrons on them were includes into the active space. The doubly occupied space was reduced by these two orbitals and the frozen core remained unchanged.

The results achieved at the MRCI level of theory with two different active spaces give notably different values of energy for the reagents CH_3 and $O_2(a^1\Delta_g)$ in the $^2A'$ term. The application of size-extensivity corrections (Davidson's, Pople's methods) permitted smoothening the difference and both results converged to a single energy point [23]. It was concluded that the smaller (MRCI (3/4)) and larger active space (MRCI (7/5)) give results regularly under- and overestimated.

Among the existing formulae for the energy correction, the Davidson correction $E_{BC} = (1 - c_0^2) \times \Delta E$ was chosen as it provides the best fit for the O_2 excitation energy and the depth of the well in the ground term ($^2A''$) with an account for vibrational zero-point energy (ZPE). Finally, the potential energy surface obtained within the MRCI (7/5) approach was selected for the further analysis as the best fit for the known thermodynamics data. The calculated energy of O_2 excitation (0.99 eV) and the well depth of CH_3O_2 in the ground state (28.6 kcal/mole taking ZPE into account) are in good agreement with the experimental values of 0.98 eV in [24] and 28.5 kcal/mole in [25] respectively. Figure 4 presents the resulting PES. The activation energy of the process (1a) is as high as 0.28 eV (0.36 eV taking ZPE into account).

Table 3 shows frequencies calculated for the optimized states. The imaginary frequency 665 cm^{-1} in the $CH_3 - O_2$ ($^2A'$) transition state corresponds to the motion in the direction of the reaction coordinate. In the ground term, the frequency 1098 cm^{-1} of the $CH_3O_2(A'')$ corresponds to the break of the C–O bond and was used in calculations of the loose variational transition state.

The COLUMBUS program package was used to perform quantum chemical calculations ([26,27]).

3.2. RRKM calculations

The rate parameters k_{1a}, k_{1b}, k_{2a}, k_{2b}, k_{1c}, k_{2c} were computed from the data of quantum chemical calculations. Microcanonical variational Rice – Ramspergen – Kassel – Marcus (RRKM) calculations were carried out using the Khimera code [15]. A microcanonical loose variational transition state was used for the rate parameters k_{2a}, k_{2c}, k_{1c} of reactions without a distinctive potential energy barrier. A rigid transition state was used for the reactions

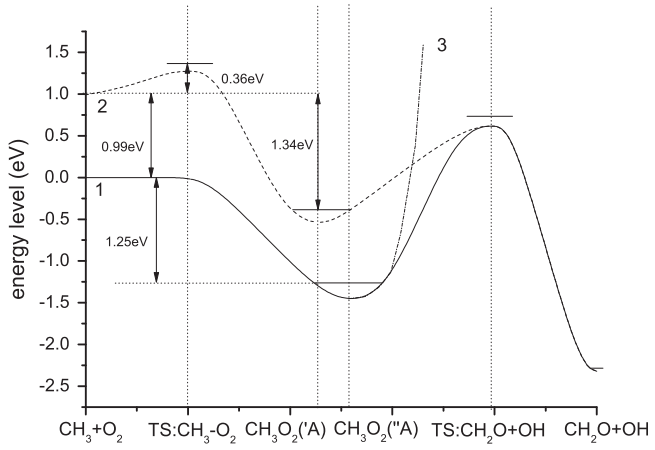

Fig. 4. Potential energy surface for the system $CH_3 + O_2$. (1) Ground term $^2A''$ corresponding to the reaction with $O_2(X^3\Sigma_g)$. (2) Excited term $^2A'$ corresponding the reaction with $O_2(a^1\Delta_g)$. (3) Crossing of terms between CH_3O_2 and the transition state to $CH_2O + OH$.

Table 3
Table of frequencies and rotational constants of species.

	CH_3	O_2	$O_2(a^1\Delta_g)$	
Frequencies (cm^{-1})	3404	1623	1596	
	3404			
	3220			
	1476			
	1474			
	455			
Rotational constants (cm^{-1})	9.56	1.44	1.44	
	9.56	1.44	1.44	
	4.78			
	CH_3O_2 ($^2A''$)	CH_3O_2 ($^2A'$)	$CH_3 - O_2(^2A'')$ (loose TS)	$CH_3 - O_2(^2A')$ (TS)
Frequencies (cm^{-1})	3259	3262	3404	3395
	3231	3252	3404	3394
	3147	3162	3220	3214
	1556	1548	1623	1485
	1545	1545	1476	1483
	1519	1497	1474	1241
	1260	1233	455	869
	1206	1203		539
	1098	1089		526
	843	973		246
	501	552		81
	192	251		665*i*
Rotational constants (cm^{-1})	0.33	0.33	$1.65 \times T^{-2}$	0.24
	0.38	0.39	$1.65 \times T^{-2}$	0.24
	1.73	1.54	$4.31 \times T^{-0.36}$	1.49
Active internal rotations (cm^{-1})			$4.31 \times T^{-0.36}$	
			$4.31 \times T^{-0.36}$	
			$4.31 \times T^{-0.36}$	
			$4.31 \times T^{-0.36}$	

k_{1a}, k_{2b}, k_{1b}. The pressure dependence was computed using the model of strong collisions with the collision efficiency factor approximated as $\beta_C = \left(\frac{1}{1+\frac{T}{190}}\right)^2$ in consistency with the expression from Ref [22] with $\frac{\Delta E_{down}}{kF_e} = 190$ K. Let us note that applicability of the strong collision approach was also verified by duplication of the simulations using master equation method [28]. These two approaches gave good coincidence for the regarded reactions in pressure and temperature ranges of our interest. The method from Troe [29] for finding the variational transition state with the Morse potential was used to compute the E-resolved rate parameter. The T- and P-resolved rate parameters of the reactions of interest were calculated using microcanonical rates of monomolecular decomposition into different sets of fragments and equilibrium constants $K_{eq}(A'') = \frac{k_{2a}}{k_{-2a}}$ and $K_{eq}(A') = \frac{k_{1a}}{k_{-1a}}$ for reactions in the ground and excited terms, respectively. To find k_{2a}, the loose variational transition state was found in the following manner. The Morse potential parameters ($D_e = 35.01$ kcal/mole, $qe = 1.726$ Å, $\beta = 3.82$ Å^{-1}) were taken from quantum chemical calculations with the corresponding classical energy of CH_3O_2 dissociation, equilibrium distance between the centers of mass of the fragments and the frequency of the C–O bond vibration (1098 cm^{-1}). The free energy of the active degrees of freedom and the zero-point energy of vibrations (ZPE) of the complex localized along the reaction coordinate q was:

$$a(q) = (a(qe) - a(\infty)) \times \exp(-\gamma(q - qe)) + a(\infty)$$
$$ZPE(q) = (ZPE(qe) - ZPE(\infty)) \times \exp(-\gamma(q - qe)) + ZPE(\infty)$$

with $\gamma = 0.75$ Å^{-1} [22]. $a(qe)$ corresponds to the free energy of the active degrees of freedom of the transition state at the geometry corresponding to the complex (CH_3O_2 particle):

$$a(qe) = -kT \ln\left(\frac{Q_{act}^{complex}}{Q_{vib}^{C-O}}\right)$$

$a(\infty)$ corresponds to active degrees of freedom of the fragments ($O_2 + CH_3$):

$$a(\infty) = -kT \ln\left(Q_{act}^{CH_3} Q_{act}^{O_2}\right)$$

The reaction coordinate $q^\dagger$ corresponding to the transition state was found as the maximum of the energy of the system:

$$q^\dagger = q : a(q) + ZPE(q) + U_{Morze}(q) + E_{cent}(q) \to \max_q$$

E_{cent} corresponds to the centrifugal potential energy associated with the two-dimensional adiabatic rotation $I_{cent} = \mu \times q^2$, where μ is the reduced mass of two fragments. At $q^\dagger$, the transition state exhibits 7 vibrations of fragments, 2 adiabatic rotations with the energy E_{cent}, and 5 active rotations: 1 overall rotation around the C–O axis and 4 active internal rotations. The rotational constants of the active rotations were calculated from the energy of the active degrees of freedom and vibrations of the transition state, so that $Q_{rot}^{act}(q^\dagger) \times Q_{vib}(q^\dagger) = \exp\left(-\frac{a(q^\dagger)}{kT}\right)$.

A similar procedure was used for the remaining reactions k_{1c} and k_{2c} with the Morse potential and the parameters of fragments taken from Ref. [21]. The potential well depth and characteristics of the complex for the reaction k_{1c} correspond to CH_3O_2 (A').

The parameters of the PES and TS for the decomposition into $CH_2O + OH$ were taken from the work [12]. The LJ parameters for CH_3O_2 ($\epsilon = 303$ K and $\sigma = 5.4$ Å) and for N_2 ($\epsilon = 82$ K and $\sigma = 3.74$ Å) were taken from [12] and [15], respectively, and used to compute cross-sections of collisions. The pressure dependence predicted by the model of strong collisions provides a good coincidence with the recommended approximation for the rate constant for oxygen in ground state [30] vs. temperature and pressure (see Figs. 5 and 6). Among the alternative reaction channels, only k_{2d} for the ground term and k_{1d} for the excited term were not taken into account as not important because of high potential energy barriers [12], inhibiting the impact of these channels at low temperature conditions.

The pressure dependence of the rate of reaction through the ground state was validated against the available experimental data (see Fig. 6). The saturation of the rate constant (high pressure limit) takes place at about 10 atm. This value is also in good agreement

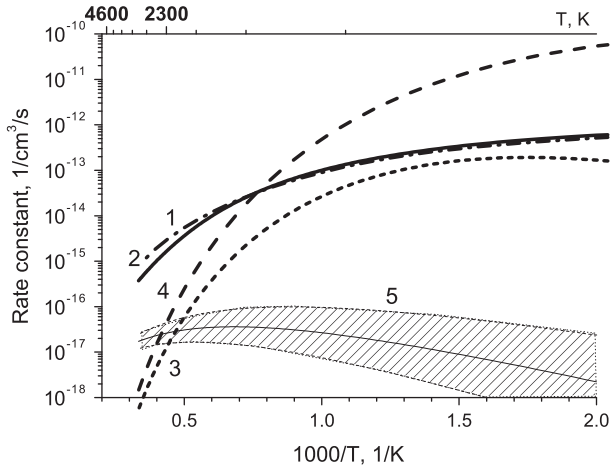

Fig. 5. Rate parameters of reactions k_{1a}, k_{2a}. $P = 1$ atm. 1, 2 and 3-reactions through ground state in accordance with the works [30], this study and [1] respectively, 4-reaction through excited state in accordance with [1], 5-reaction through excited state in accordance with this study.

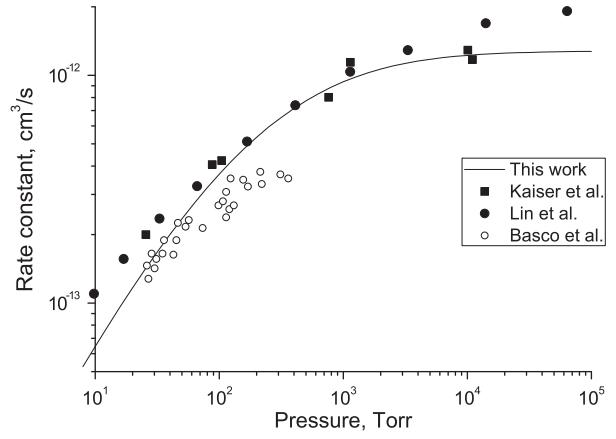

Fig. 6. Dependence of rate parameter of the reaction k_{2a} upon pressure at $T = 300$ K in N_2 calculated in this study. Comparison with works Kaiser et al. [31], Lin et al. [12], and Basco et al. [32].

Table 4
Rate parameters of reactions from different sources, $P = 1$ atm.

	$A\left(\frac{cm^3}{s}\right)$	n	E_a (kcal/mole)
k_{1a}	2.76×10^{-7}	−2.71	8.61
k_{2a}	1.17×10^{5}	−5.73	4.12
k_{1b}	5.76×10^{-17}	1.63	6.9
k_{2b}	6.85×10^{-20}	2.09	12.11
k_{1c}	1.70×10^{-20}	2.68	6.66
k_{2c}	7.74×10^{-14}	0.71	26.96

with the values used in other works (see discussion in [12]). The results obtained for the reaction through the ground state $^2A''$ may be considered as the validation of the data of ab initio calculations.

Figure 5 and Table 4 present the dependence of the rate of association reaction via excited state $^2A'$ vs. temperature and the parameters of rate constant approximation in the quasi-Arrhenius form. The figure also includes the rate approximation used in the work [1]. The confidence interval of the calculation (dashed area) was estimated from the characteristic value of the error of threshold calculation ±2 kcal/mole.

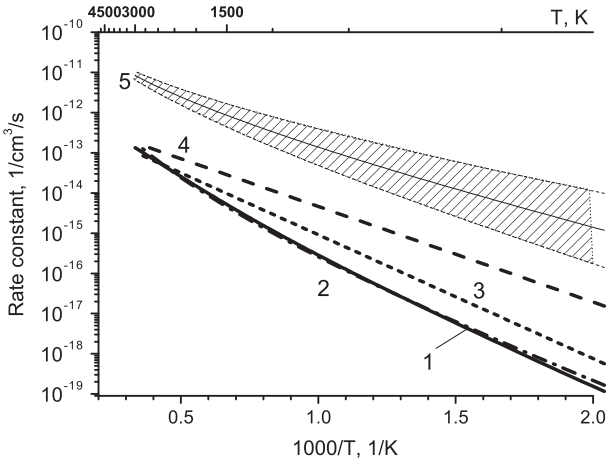

Fig. 7. Rate parameters of reactions k_{1b}, k_{2b}. $P = 1$ atm. 1, 2 and 3-reactions through ground state in accordance with the works [12], this study and [1] 4-reaction through excited state in accordance with the study [1], 5-reaction through excited state in accordance with this study.

The reaction for the singlet state is several orders of magnitude slower than the reaction of the triplet state at the characteristic pressure 1 atm. This effect can be explained by the appearance of an energy barrier in the reaction path and by the high probability for CH_3 and $O_2(a^1\Delta_g)$ reaction directly into CH_2O and OH, avoiding stabilization of the way into the methylperoxy radical (CH_3O_2). The reaction rate is three orders of magnitude lower than that from [1], where intuitive suggestions about the PES behavior were used in calculations within the "vibronic terms" approach.

In Fig. 7 the rate constant of reactions k_{1b}, k_{2b} is shown as a function of temperature at atmospheric pressure. The results are compared with the data of ab initio calculations [12] and work [1]. Our calculations demonstrate a strong effect of the potential energy surface features on the rate behavior at low temperatures. Comparison of the three possible channels for the reaction with excited oxygen shows that the stabilization phenomena of the intermediate complex becomes significant at pressures greater than 300 atm. Therefore channels k_{1b} and k_{1c} are principal reactions in wide range of pressures and temperature.

Table 4 gives parameters of the quasi-Arrhenius approximation of reactions for CH_2O for the $^2A''$ and $^2A'$ terms, respectively.

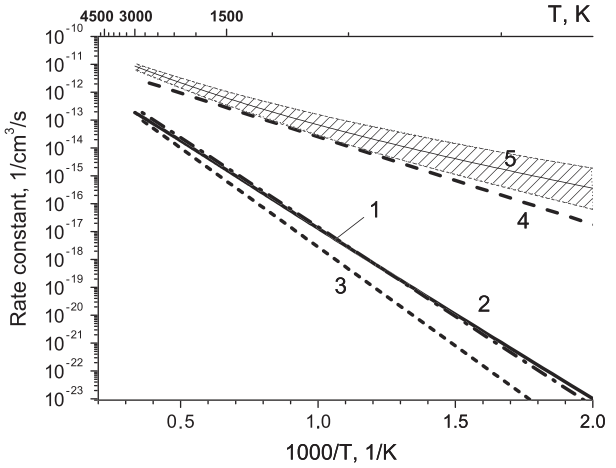

Fig. 8. Rate parameters of reactions k_{1c}, k_{2c}. $P = 1$ atm. 1, 2 and 3-reactions through ground state in accordance with the works [21], this study and [1] 4-reaction through excited state in accordance with the study [1], 5-reaction through excited state in accordance with this study.

As was mentioned in the works [12] and [11], the production of CH_2O and OH requires PES hopping with a high transition probability between the $^2A'$ and $^2A''$ states. Using the results of this study and the parameters of the saddle points from [11], we came to the conclusion that the rate constant of reaction to CH_2O for the excited state is higher than that for the ground one at low and moderate pressures.

Figure 8 provides a comparison of the rates of the reactions k_{1c} and k_{2c}. The rate of the reaction k_{1c} is significantly greater than the reaction through the ground term because of the difference in the endothermicity of the reactions. The graphs also present a comparison of the temperature dependence of the calculated rate parameters with the corresponding data from other works. The comparison of the reaction rate of k_{2c} with the corresponding data from the Ref. [21] shows that the rate for the triplet state is well reproduced by our model. A comparison of the rate k_{1c} with the curve from [1] exhibits a coincidence, which probably indicates that the vibronic term approach is justified in this case.

4. Discussion

The initial analysis of the importance of reactions (see Section 1) and of the input of different processes to $O_2(a^1\Delta_g)$ losses was carried out based on the sub-mechanism developed in [1]. However, ab initio calculations show that the absolute values of the rates and branching ratios between the channels in the reaction of excited oxygen with the methyl radical should be corrected. In general, the correction may lead to the change of the conclusion on the singlet oxygen effect on the oxidation initiation. Figure 9 demonstrates the initial stages of the kinetic sub-mechanism involving $O_2(a^1\Delta_g)$. The channels (k_1') and (k_2') represent the sum of chain propagation reactions k_{1c}, k_{1d} and k_{2c}, k_{2d} respectively. Other channels (k_{1a}), (k_{2a}), and (k_3) are oxidation initiation with the involvement of methane and the methyl radical. Quenching of the excited state of the methyl peroxy radical is also included into the scheme. Three principal pathways can be constructed from the point of view of excited oxygen losses:

I. Transfer of electronic excitation to gas heating via reactions $(k_{1a}) \rightarrow (quenching) \rightarrow (k_{-2a})$.
II. Initiation of methane oxidation in the reaction (k_3).
III. Initiation of a branched chain oxidation mechanism in the reactions (k_{1b}) and (k_{2b}).

The loss of $O_2(a^1\Delta_g)$ by the pathway I is just the transfer of the energy of electronic excitation of $O_2(a^1\Delta_g)$ to a translational degree of freedom. This way can be considered a fruitless way in comparison with the pathways II and III, along which excitation energy goes directly for the acceleration of chemical transformations. The total flux of excited oxygen by the first, second, and third pathway is

$$J_I = v_{-2}[CH_3O_2] \tag{5}$$

$$J_{II} = v_3[O_2(a^1\Delta_g)] \tag{6}$$

$$J_{III} = v_1'[CH_3O_2^*] + v_2'[CH_3O_2] \tag{7}$$

where $v_3 = k_3[CH_4]$. See index notation on the Fig. 9.

Assuming a quasi-steady-state concentration for $CH_3O_2(^2A',^2A'')$, the following evident expressions for the excited oxygen flow ratio between the pathways I, II and III can be obtained:

$$\frac{J_{III}}{J_I} = \frac{v_2'}{v_{-2}} + \frac{v_1'}{v_q}\left(1 + \frac{v_2'}{v_{-2}}\right) \tag{8}$$

$$\frac{J_{II}}{J_I} = \frac{v_3}{v_1}\left(1 + \frac{v_2'}{v_{-2}}\right)\left(1 + \frac{v_1' + v_{-1}}{v_q}\right) \tag{9}$$

According to Eq. (8), the efficiency of acceleration of branched chain oxidation by singlet oxygen is independent of the rate of reaction $CH_3 + O_2(^1\Delta_g) \rightarrow CH_3O_2(^2A'')$. Nevertheless, according to Eq. (9), the rate of this reaction does play a significant role in determining the efficiency of the initiation reaction k_3.

Due to absence of experimental results for low-temperature combustion stimulated by $O_2(a^1\Delta_g)$ the examination given can be applied to interpretation of the simulations results based on different kinetic mechanisms. Diminishing of the rate constant of the reaction (k_{1a}) in accordance with calculations of this study leads at first glance to paradoxical result in framework of the mechanism [1], namely, to the acceleration of the overall oxidation rate. On Fig. 10 the time dependence of mixture temperature is presented. Simulations were carried out for stoichiometric air–methane mixture at pressure 1 atm and initial temperature 900 K. Initial concentration of singlet oxygen was $[O_2(a^1\Delta_g)]/[O_2] = 0.05$. The sub-mechanism of $O_2(a^1\Delta_g)$ reactions from the work [1] was used.

The presence of $O_2(a^1\Delta_g)$ reduces ignition time twice and clearly indicates that singlet oxygen can enhance process rate significantly. However, the reduction of the rate constant of reaction (k_{1a}) in accordance with the calculations performed in this study makes the process even faster. The induction time estimated to this

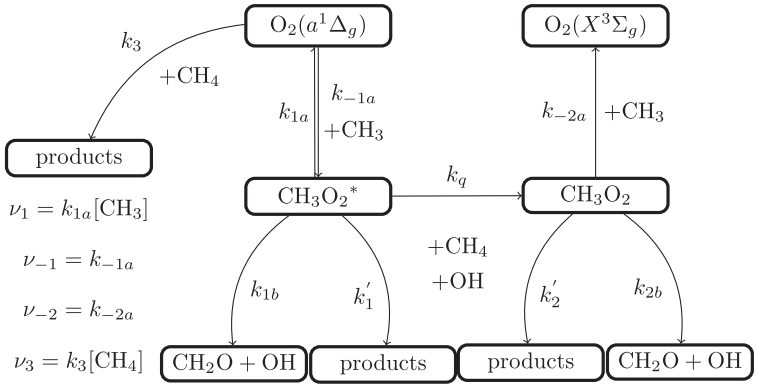

Fig. 9. Diagram of initiation reactions with $O_2(a^1\Delta_g)$ participation.

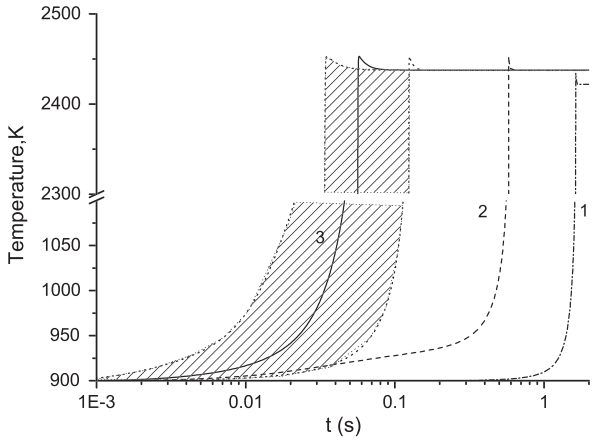

Fig. 10. Time dependence of the temperature with different rate parameter values. T_{ini} = 900 K, $[O_2(a^1\Delta_g)]/[O_2]$ = 0.05 1-calculation without $O_2(a^1\Delta_g)$, 2 and 3-calculation with $O_2(a^1\Delta_g)$ based on paper [1] mechanism and with corrected rate of reaction (k_{1a}).

Table 5
Main species flows with rate parameters from Starik et al. [1], T_{ini} = 800 K, P = 1 atm, t = 1 ms.

Reaction name	$O_2(a^1\Delta_g)$	CH_3	CH_3O_2
$CH_3 + O_2(a^1\Delta_g) \rightarrow CH_3O_2$	1	1	0
$CH_3O_2 \rightarrow CH_3 + O_2$	0	0	1
$CH_3O_2 + CH_4 \rightarrow CH_3O_2H + CH_3$	0	0	0

study is two orders of magnitude less than the induction time without singlet oxygen. This unusual result can be explained taking into account the influence of the variation of rate constant on the energy distribution of excited oxygen over different channels I, II and III and peculiarities of the used sub-mechanism [1]. In the sub-mechanism used, the methyl peroxy radical is present only in the ground state ($^2A''$). This corresponds to the proposal of a very high quenching rate v_q of the process CH_3O_2 ($^2A'$) + M → CH_3O_2 ($^2A''$) + M, i.e. $v_q \gg v_1, v_{-1}, v_1'$. This means (see Eqs. (8) and (9)) that a decrease in the rate of reaction (k_{1a}) does not affect the distribution of excited oxygen flow between the initiation of branched oxidation (III) and energy relaxation (I). However, it simultaneously leads to the preferable consumption of excited oxygen in the channel of oxidation initiation (II) in comparison with energy relaxation to heat. In other words, a decrease in the rate (k_{1a}) reduces the rate of energy pumping to the translational degree of freedom via the reaction k_q and redistributes excited oxygen energy towards the activation of the chain initiation process. As a consequence, temperature rise (Fig. 10) at the early stages of the oxidation process takes place within the original kinetic mechanism [1].

Tables 5 and 6 show flows of the main species for two cases, with the rate constant for the process (k_{1a}) according to [1] and the rate parameter computed in this study. The results are shown for an initial temperature of 800 K at the time $\tau \sim 10^{-3}$.

Table 6
Relative consumption rate of the main species with rate parameters from this study, T_{ini} = 800 K, P = 1 atm, t = 1 ms.

Reaction name	$O_2(a^1\Delta_g)$	CH_3	CH_3O_2
$CH_3 + O_2(a^1\Delta_g) \rightarrow CH_3O_2$	0.00	0.00	0
$CH_3 + O_2(a^1\Delta_g) \rightarrow CH_2O + OH$	0.66	0.60	0
$CH_3 + O_2(a^1\Delta_g) \rightarrow CH_3O + O$	0.27	0.25	0
$CH_4 + O_2(a^1\Delta_g) \rightarrow CH_3 + HO_2$	0.07	0.05	0
$CH_3O_2 \rightarrow CH_3 + O_2$	0	0	0
$CH_3O_2 + CH_3 \rightarrow 2CH_3O$	0	0	0.96

According to Table 5, all CH_3O_2 produced by singlet oxygen recombines back to CH_3, as these two species are in a quasi-equilibrium. Thus, $O_2(a^1\Delta_g)$ only converts CH_3 to CH_3O_2 and does not give new radicals. The result of the sequence

$$O_2(a^1\Delta_g) + CH_3 \rightarrow CH_3O_2 \rightarrow CH_3 + O_2$$

is just quenching of $O_2(a^1\Delta_g)$.

The modified mechanism (Table 6) includes competitive reactions (k_{1a}, k_3, k_{1b}) leading to the creation of additional CH_3 radicals by singlet oxygen. The amount of additional CH_3 radicals is sufficient for the initiation of a reaction via the following branch:

$$CH_4 \rightarrow CH_3 \rightarrow CH_3O \rightarrow CH_2O \rightarrow HCO \rightarrow CO \rightarrow CO_2$$

In this mechanism, the main role of $O_2(a^1\Delta_g)$ is the production of new radicals rather than pumping of excitation energy into heat.

5. Conclusions

The potential energy surface of the reaction $CH_3 + O_2(a^1\Delta_g)$ was investigated with the degree of accuracy sufficient for analysis of the kinetic peculiarities of methane oxidation at low temperatures $T < 1000$ K. It was found that the threshold of the reaction is 8.5 kcal/mole, which is only 3.4 kcal/mole above the barrier to another channel leading to the products CH_3O and O. Therefore, formation of CH_2O and CH_3O are the most important channels of the reaction. The results of the kinetics simulations strongly depend upon features of the $O_2(a^1\Delta_g)$ sub-mechanism and the branching ratio between the channels of the reaction. Rate constants of the reactions with participation of $O_2(a^1\Delta_g)$ were calculated. It was established that the peculiarities of the process mentioned above lead to the effective transfer of energy of electronic excitation to generation of radicals and acceleration of the oxidation. To clarify the situation with effect of $O_2(a^1\Delta_g)$ on the combustion of methane at low temperatures, further high-level accuracy investigations of the other process involving the excited methyl peroxy radical (chain propagation and quenching) should be performed.

Acknowledgments

The authors thank Prof. S. Umanskii for the helpful discussion concerning this work. The potential energy surface for the $CH_3 + O_2$ system was calculated using computational resources of the MCC NRC "Kurchatov Institute" cluster (http://computing.kiae.ru/).

References

[1] A.M. Starik, V.E. Kozlov, N.S. Titova, Combust. Flame 157 (2010) 313–327.
[2] A. Starik, N. Titova, Kinet. Catal. 44 (2003) 28–39.
[3] N.A. Popov, I.A. Kossyi, in: 45th AIAA Aerospace Sciences Meeting and Exhibit.
[4] T. Ombrello, S.H. Won, Y. Ju, S. Williams, Combust. Flame 157 (2010) 1916–1928.
[5] L. Wu, A.A. Fridman, A.Y. Starikovskiy, in: 20th ESCAMPIG, 13–17 July 2010.
[6] A.M. Starik, N.S. Titova, Kinet. Catal. 47 (2006) 487–496.
[7] E. Ranzi, T. Faravelli, P. Gaffuri, A. Sogaro, Combust. Flame 102 (1995) 179.
[8] V.E. Kozlov, A.M. Starik, N.S. Titova, Combust. Explos. Shock Waves 44 (2008) 371–379.
[9] A.M. Starik, P.S. Kuleshov, N.S. Titova, Tech. Phys. 53 (2008) 235–243.
[10] D. Frank-Kamenetskii, Diffusion and Heat Transfer in Chemical Kinetics, Plenum Press, 1969.
[11] S.P. Walch, Chem. Phys. Lett. 215 (1993) 81–86.
[12] R. Zhu, C.-C. Hsu, M. Lin, J. Chem. Phys. 115 (2001) 195–203.
[13] M. Deminsky, I. Kochetov, A. Napartovich, S. Leonov, Int. J. Hypersonics 1 (2010) 209.
[14] M. Deminsky, I. Chernysheva, S. Umanskii, M. Strelkova, A. Baranov, I. Kochetov, A. Napartovich, T. Sommerer, S. Saddoughi, J. Herbon, B. Potapkin, Russ. J. Phys. Chem. A 32 (2013), in press.
[15] M. Deminsky, V. Chorkov, G. Belov, I. Cheshigin, A. Knizhnik, E. Shulakova, M. Shulakov, I. Iskandarova, V. Alexandrov, A. Petrusev, I. Kirillov, M. Strelkova, S. Umanski, B. Potapkin, Comput. Mater. Sci. 28 (2003) 169.

[16] A. Lebedev, M. Okun, A. Baranov, M. Deminsky, B. Potapkin, Phys. Chem. Kinet. Fluid Dyn. 10 (2010).
[17] A.V. Lebedev, M.V. Okun, V.A. Chorkov, P.M. Tokar, M. Strelkova, J. Math. Chem. (2012).
[18] V.S. Arutiunov, V.J. Basevitch, V. Vedeneev, Russ. Chem. Rev. 65 (1996) 221.
[19] M. Dallos, H. Lischka, E.V. do Monte, M. Hirsh, W. Quapp, J. Comput. Chem. 23 (2002) 576–583.
[20] C.J. Cobos, H. H, K. Luther, A.R. Ravishankara, J. Troe, J. Phys. Chem. 89 (1985) 4332–4338.
[21] C.-L. Yu, C. Wang, M. Frenklach, J. Phys. Chem. 99 (1995) 14377–14387.
[22] M. Keiffer, M.J. Pilling, M.J.C. Smith, J. Phys. Chem. 91 (1987) 6028–6034.
[23] S.R. Langhoff, E.R. Davidson, Int. J. Quantum Chem. 8 (1974) 61–72.
[24] B. Rosen (Ed.), Spectroscopic Data Relative to Diatomic Molecules, Pergamon, Oxford, 1970.
[25] M.W. Chase, C.A. Daives, J.R. Downey, D.J. Frurip, R.A. McDonald, A.N. Syverud, J. Phys. Chem. Ref. Data 14 (1985) (Supplement No. 1).
[26] H. Lischka, R. Shepard, F.B. Brown, I. Shavitt, Int. J. Quantum Chem., Quantum Chem. Symp. 15 (1981) 91.
[27] T. Helgaker, H.J.A. Jensen, P. Jrgensen, J. Olsen, K. Ruud, H. gren, T. Andersen, K.L. Bak, V. Bakken, O. Christiansen, P. Dahle, E.K. Dalskov, T. Enevoldsen, H. Heiberg, H. Hettema, D. Jonsson, S. Kirpekar, R. Kobayashi, H. Koch, K.V. Mikkelsen, P. Norman, M.J. Packer, T. Saue, P.R. Taylor, O. Vahtras.
[28] J.R. Barker, Int. J. Chem. Kinet. 33 (2001) 232.
[29] M. Quack, J. Troe, Ber. Bunsenges. Phys. Chem. 81 (1977) 329–337.
[30] D.L. Baulch, C. Bowman, C.J. Cobos, R.A. Cox, T. Just, J.A. Kerr, M.J. Pilling, D. Stocker, J. Troe, W. Tsang, R.W. Walker, J. Warnatz, J. Phys. Chem. Ref. Data 34 (2005) 757–1397.
[31] E.W. Kaiser, J. Phys. Chem. 97 (1993) 11681–11688.
[32] N. Basco, D.G.L. James, F.C. James, Int. J. Chem. Kinet. 4 (1972) 129–149.

Please cite this article in press as: A.V. Lebedev et al., Combust. Flame (2012), http://dx.doi.org/10.1016/j.combustflame.2012.11.020